

The Expansion of the Young Supernova Remnant 0509-68.7 (N103B)

Brian J. Williams ¹, William P. Blair ², Kazimierz J. Borkowski ³, Parviz Ghavamian ⁴, Sean P. Hendrick ⁵, Knox S. Long⁶, Robert Petre¹, John C. Raymond⁷, Armin Rest⁶, Stephen P. Reynolds³, Ravi Sankrit⁶, Ivo R. Seitenzahl⁸, and P. Frank Winkler⁹ ¹ NASA Goddard Space Flight Center, Greenbelt, MD 20771, USA; brian.j.williams@nasa.gov Johns Hopkins University, Baltimore, MD, USA ³ North Carolina State University, Raleigh, NC, USA Towson University, Towson, MD, USA ⁵ Millersville University, Millersville, PA, USA ⁶ Space Telescope Science Institute, Baltimore, MD, USA ⁷ Harvard-Smithsonian Center for Astrophysics, Cambridge, MA, USA ⁸ University of New South Wales, Australian Defence Force Academy, Canberra, ACT 2600, Australia Middlebury College, Middlebury, VT, USA Received 2018 August 17; revised 2018 September 7; accepted 2018 September 8; published 2018 September 25

Abstract

We present a second epoch of *Chandra* observations of the Type Ia Large Magellanic Cloud supernova remnant (SNR) 0509-68.7 (N103B) obtained in 2017. When combined with the earlier observations from 1999, we have a 17.4 year baseline with which we can search for evidence of the remnant's expansion. Although the lack of strong point source detections makes absolute image alignment at the necessary accuracy impossible, we can measure the change in the diameter and the area of the remnant, and find that it has expanded by an average velocity of 4170 (2860, 5450) km s⁻¹. This supports the picture of this being a young remnant; this expansion velocity corresponds to an undecelerated age of 850 years, making the real age somewhat younger, consistent with results from light echo studies. Previous infrared observations have revealed high densities in the western half of the remnant, likely from circumstellar material, so it is probable that the real expansion velocity is lower on that side of the remnant and higher on the eastern side. A similar scenario is seen in Kepler's SNR. N103B joins the rare class of Magellanic Cloud SNRs with measured proper motions.

Key words: ISM: individual objects (SNR 0509-68.7) – ISM: supernova remnants – proper motions

1. Introduction

The supernova remnant (SNR) 0509-68.7 is one of the most luminous X-ray sources in the Large Magellanic Cloud (LMC), despite being only $\sim 30''$ in diameter (about 3.6 pc at the distance of the LMC). 10 The Advanced Satellite for Cosmology and Astrophysics (ASCA) observations of N103B were presented in Hughes et al. (1995), who first identified the remnant as the result of a Type Ia supernova (SN), a conclusion that has been confirmed by several authors (Lewis et al. 2003; Badenes et al. 2009; Lopez et al. 2011; Yang et al. 2013). A single light echo was detected by Rest et al. (2005), who derived an age of 860 years for the remnant, broadly consistent with its small size (remnants of comparable size in the LMC are <1000 years old). Ghavamian et al. (2017) used integral field spectroscopy of the Balmer-dominated shocks to detect broad $H\alpha$ emission having a width as high as 2350 km s⁻¹. They derive an age of 685 years, assuming that the remnant is in the Sedov phase. Recently obtained light echo spectroscopy has shown that the spectrum of the light echo is consistent with an SN Ia origin (A. Rest 2018, in preparation).

In Williams et al. (2014, henceforth W14), we used Spitzer imaging and spectroscopy to show that the remnant appears to be interacting with dense circumstellar material (CSM; $n_0 \sim 10 \text{ cm}^{-3}$),

remarkably similar to the densities observed in Kepler's SNR by Williams et al. (2012). We suggested there that N103B is an LMC older cousin of Kepler's SNR, and thus far, these two remnants are the only two members of the class of Type Ia remnants interacting with dense CSM hundreds of years after the explosion. Li et al. (2017) presented optical imaging and spectroscopy of N103B, concluding that the lack of emission in the eastern half of the remnant is caused by the asymmetric distribution of the CSM due to the high proper motion of the progenitor binary system toward the west.

In this Letter, we report a new epoch of X-ray observations with *Chandra* from 2017, which we use to measure the expansion of the remnant over a 17.4 year baseline. While X-ray proper motion measurements of Galactic remnants are commonplace, only a few remnants in the Magellanic Clouds have a high enough expansion velocity to allow for an expansion measurement. One example of this is the young Type Ia remnant 0509-67.5, which has had expansion measurements reported in the literature in both optical (Hovey et al. 2015) and X-ray (Helder et al. 2010; Roper et al. 2018) wavelengths. As another example, L. Xi et al. (2018, in preparation) have used Chandra observations of 1E0102.2-7219 in the Small Magellanic Cloud to observe the proper motions in that remnant.

This Letter is organized as follows. In Section 2, we detail the X-ray observations and data reduction, and the attempts to align the two epochs to a common coordinate system. In Section 3, we report the results of our measurements and discuss their interpretation. Section 4 serves as a summary of our findings. Throughout this Letter, we convert our

This remnant is often labeled as N103B, though this labeling is incorrect. "N103B" refers to a nebula first discovered at optical wavelengths by Henize (1956), but that nebula is not the SNR (it is an H II region several arcminutes in diameter to the SW of the remnant). SNR 0509-68.7 was first identified in radio waves by Mathewson & Clarke (1973). Nonetheless, the N103B misnomer has stuck, and is more widely associated with this remnant than the original nebula, so we use the name for the remainder of this Letter.

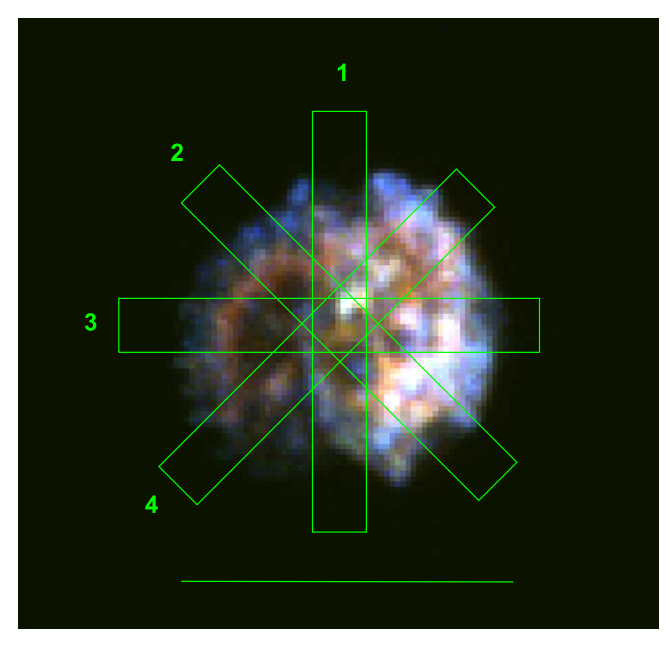


Figure 1. Chandra X-ray image of N103B, with 0.5–1.2 keV in red, 1.2–2.0 keV in green, and 2.0–7.0 keV in blue, overlaid with our four profile extraction regions, as described in the text. Each region is 10 pixels wide, where a pixel is the native *Chandra* pixel scale of 0."492. The scale bar at the bottom is 30" in length.

measurements made in image units to the more useful physical quantity of km s⁻¹, taking advantage of the known distance to the LMC of 50 kpc (Pietrzynski et al. 2013).

2. Observations

We conducted a new epoch of Chandra imaging observations of N103B in the spring of 2017, with a total of 400 ks spread over 12 separate observations between March 20 and June 1. We used the ACIS-S array for these observations, placing the remnant (only $\sim 30''$ in diameter) close to the center of the optical axis of the telescope on the S3 chip, where Chandra's spatial resolution is best. The 1.7–7 keV image from these 2017 observations is shown in Figure 1. To measure the expansion of the remnant, we compared our 2017 observations with the earliest epoch: a 1999 December 4 observation for 40 ks (PI: G. Garmire). Our method for fitting the proper motion involves shifting one epoch with respect to another, accounting for the uncertainties in each epoch. This technique is described more fully in Williams et al. (2017) and Katsuda et al. (2008), but briefly, we extract brightness profiles from the image in units of counts, with the square root of the number of counts as the uncertainty on each pixel. One epoch, generally the second, is used as the "reference" epoch, with the other epoch shifted until the total χ^2 value is minimized.

The effect that we are measuring is quite small (sub-arcsecond, see Section 3), so we took care to minimize or eliminate any potential sources of systematic uncertainty in our measurements. First, we opted not to combine the data from our 12 observations into a single event file, as this could create biases in the resulting FITS files at the sub-pixel level which would be difficult, if not impossible, to quantify. For our "reference" frame, we used the deepest single observation from our 2017 observations: a 60 ks observation (ObsID 19923) begun on April 26. These data, along with the 1999 data (which combine for a time baseline of 17.4 years), were both processed

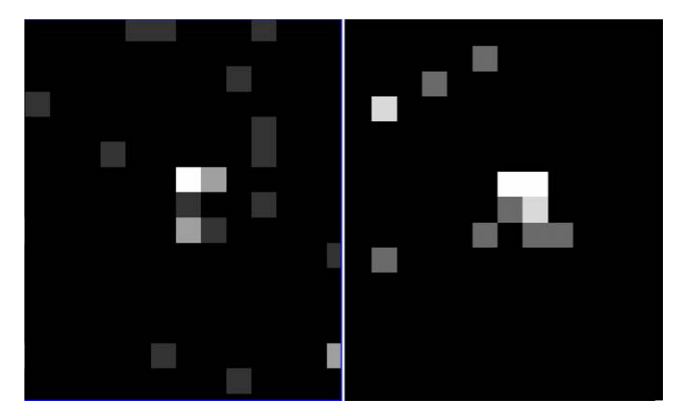


Figure 2. One of the sources detected in the field of view, located approximately 1'.5 from the remnant. The counts image from the 1999 observation is shown on the left, while the 2017 image is shown on the right. Each image is shown at the native *Chandra* pixel scale of 0''.492. The source contains 16 counts in the 1999 data and 25 counts in the 2017 data.

in identical fashion with the *chandra_repro* script in CIAO version 4.9 (using version 4.7.3 of the *CalDB*).

2.1. Image Registration and Alignment

The standard methods for aligning images in the world coordinate system (WCS) for a proper motion measurement involve either registering point sources detected in the image with known sources from external catalogs or aligning on common point sources within the images from each epoch, allowing for at least a relative alignment. While the former method is obviously preferred, X-ray analysis often relies on the latter, due to the relative paucity of point sources in the X-ray band with known optical counterparts. N103B is an LMC remnant; however, its location (R.A. = $05^{h}08^{m}59^{s}$, decl. = $-68^{\circ}43'34''$, J2000.) is well outside the main bar of the LMC and unfortunately, the number of point sources in the field of view is quite low. We restricted ourselves to point sources on the S3 chip (within 4' of the remnant), because Chandra's point-spread function (PSF) degrades quickly as a function of off-axis angle.

To search for point sources in the events files from the two epochs, we first used the CIAO task *wavdetect*, as recommended by the *Chandra X-ray Center*. This task "found" a few dozen point sources in the image, but most were false positives. A relatively simple search by eye confirmed that only five of these sources were real and detected in both epochs. Using these five sources as input, we created a transformation matrix file using the *wcs_match* task, then used *wcs_update* to align the 1999 epoch 1 image to the 2017 epoch 2 image.

Unfortunately, the results of this alignment were not accurate enough for a robust measurement. When we attempted to measure the proper motion of the leading edge of the emission (presumably the shock front), our results varied substantially, with results approaching 15,000 km s⁻¹ in some places and *negative* 5000 km s⁻¹ in others! We re-did the alignment using another CIAO tool, *srcextent*, but the results were similarly wildly varying depending on location within the remnant.

Upon further inspection, we concluded that most of the point sources (all but one) used for alignment in both the *wavdetect* and *srcextent* methods do not have a strong enough detection for these algorithms to fit a PSF and determine an accurate location. As an example of what we mean by this, we show one of our sources in Figure 2. That this source is real is

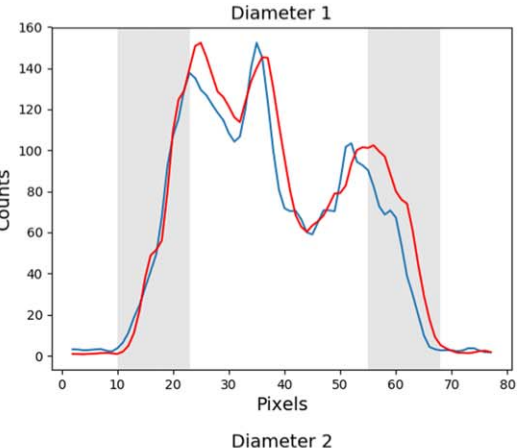
unquestionable, and it appears in nearly the same location in both epochs. But Figure 2 shows why any localization algorithms would not be able to report a location to the accuracy that we require. This source contains only about 15–25 photons in total, depending on the epoch, which is nowhere near enough counts to get a two-dimensional centroid accurate to the sub-arcsecond level. For example, using Equation (13) from Kim et al. (2007), we find positional uncertainties in the source shown in Figure 2 of 0.44 and 0.35 in the first and second epoch, respectively. The accuracy of the location is of utmost importance here, as the signal we are searching for is so small. For reference, even with *Chandra* and a time baseline of 17.4 years, a 5000 km s⁻¹ blast wave at a distance of 50 kpc would move only \sim 0.37 during that time, or about 3/4 of a *Chandra* pixel.

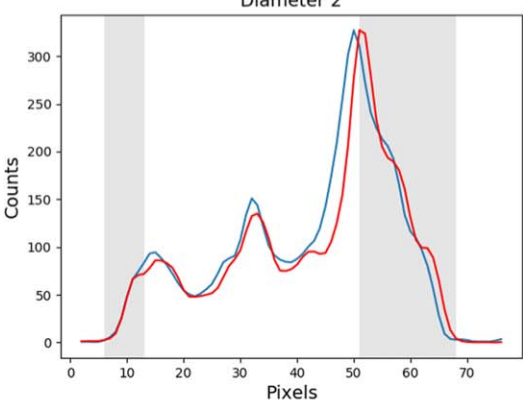
We explored other options as well. There are a few knots of emission near the center of the remnant that could, in principle, serve as markers for alignment. However, not only are these sources relatively diffuse (several arcseconds in extent), there is also no way of knowing that these knots do not have their own motion or slightly varying surface brightness profiles over the 17.4 years of evolution of the remnant. We also opted not to use CIAO's sub-pixelization algorithms. There is too much potential for the introduction of a significant systematic uncertainty by reducing the pixel size on the same length scale as the signal that we are trying to measure.

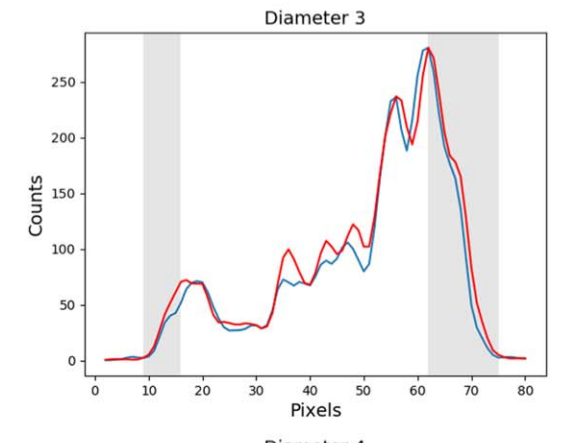
Ultimately, the uncertainties involved in obtaining image registration down to a fraction of a pixel led us to focus on measuring one thing that does not require knowledge of the WCS registration: the remnant's diameter along various axes. As we show below, we chose to measure the diameter of N103B in four directions (see Figure 1), effectively forming two orthogonal cardinal coordinate systems. Before making these measurements, we made one final filtering of the data. The ACIS array has suffered significant degradation at low energies due to contaminant buildup since launch. At low energies, the difference between the effective area in 1999 and 2017 is quite significant. Thus, we only considered counts at energies above 1.7 keV (up to 7 keV), high enough to ensure a nearly similar effective area to the 1999 observations while still capturing the strong $\sim \! 1.8 \, \text{keV}$ Si $\mathrm{K}\alpha$ line.

3. Measurements and Discussion

We measured the diameter of the remnant using the radial profiles (obtained by using *projection* regions in ds9) along four "diameter" regions, shown in Figure 1. These regions sample the entire brightness profile of the remnant along diameters covering position angles 0–180, 45–225, 90–270, and 135–315. We made no attempt to scientifically define a center of the remnant, because the site of the explosion is unknown. We simply drew the diameter regions to run through the geometric center of the circular structure of N103B. To obtain enough signal for a robust profile, each region is 10 pixels wide, or $\sim 5''$. The normalized brightness profiles extracted from each diameter in the two epochs are shown in Figure 3. We are not concerned with the small changes in internal structure, only the change in the diameter of the remnant as marked by the sharp rise of the shock front. To do







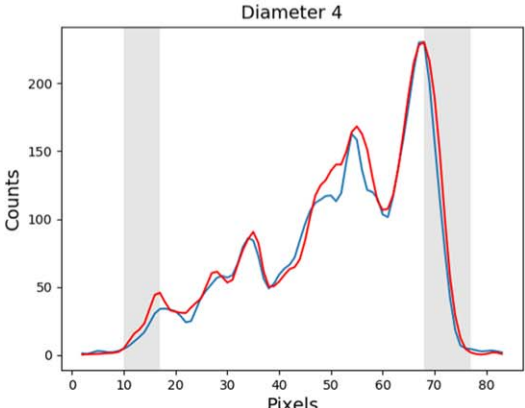


Figure 3. Brightness profiles of epoch 1 (1999) in blue and epoch 2 (2017) in red for diameter regions 1 and 2, normalized for display purposes. The gray shaded regions mark the regions in which the fits were performed. The normalization was adjusted for each shaded region. The profiles run north-to-south for region 1 and east—west (left to right) for regions 2–4.

¹¹ From the point of view of image transformation, it is a simple matter to simply arbitrarily define any point one wishes as a "fixed source" for alignment between the two epochs.

Table 1 Expansion Velocities for N103B

Region	Mean v_s (km s ⁻¹)	Lower Limit	Upper Limit
1	5360	4080	6570
2	4070	3140	4940
3	4280	3320	5250
4	2990	910	5030
Average	4170	2860	5450

Note. Mean v_s is total expansion of the shock front along each diameter region, divided by two, as described in the text. Distance is assumed to be 50 kpc. The lower and upper limits include both statistical and systematic uncertainties, as described in the text. All results are reported to the nearest 10 km s^{-1} .

this, we measure the shift in the shock front on both the left side and right side of the profiles separately (these "fit" regions are marked by shaded gray areas in Figure 3). The relative normalization of the peak of emission is tailored to each of these regions. Taking into account the uncertainty on each profile data point (not shown in the figures for display purposes), we shift epoch 1 with respect to epoch 2 on a fine grid of 0."0048 resolution elements (~0.01 *Chandra* pixels).

The total expansion velocity in each region is simply reported as the average of the two values that we measure, one from each side of the remnant. As can be seen from the Figures, the rise in the brightness profiles marking the edge of the shock front is generally fairly consistent between epochs. A few exceptions exist, such as the left (east) sides of regions 3 and 4. Nonetheless, those were included in the fitting procedure, and simply resulted in increased uncertainties in those regions. In a few places, such as the left side of region 1, epoch 2 is interior to epoch 1, leading to a negative shock velocity, almost certainly due to a coordinate registration error, as discussed above. However, the strength of this fitting procedure is that the change of the diameter of the remnant does not depend on this. For example, in the case of diameter region 1, we "measure" a shock velocity of $-4070 \,\mathrm{km \, s^{-1}}$ for the left (north) side of the emission, and an incredible (and almost certainly unphysical) 14,840 km s⁻¹ for the right (south) side. However, the average of these two is 5360 km s⁻¹, the value reported in Table 1, which should be robust even in light of uncertainties in the image registration.

For the uncertainties, we measure both statistical and systematic error terms. The statistical uncertainties come from the fits themselves: we report the best fit as the shift in which the value of χ^2 is minimized, and take as the 90% confidence limits the value of the shift in each direction where χ^2 has risen by 2.706. For the systematic uncertainties, the typical reported values, such as those in Katsuda et al. (2013), of the registration uncertainties in aligning the images are irrelevant for our purposes. Instead, we found that varying the choice of fit region for each shock front, marked by the shaded gray areas, resulted in slightly different values for the shock velocity. These errors were generally small, usually a few tens of km s⁻¹, and are dwarfed by the statistical uncertainties on the fit. Nonetheless, we include both uncertainties, added linearly, in our results reported in Table 1. Our values for the average expansion velocity range from 2990 to 5360 km s⁻¹, with a mean expansion velocity of 4170 km s⁻¹, with lower and upper limits of 2860 and 5450, respectively.

As a final "sanity check" on the expansion of N103B, we conducted an entirely different and independent experiment.

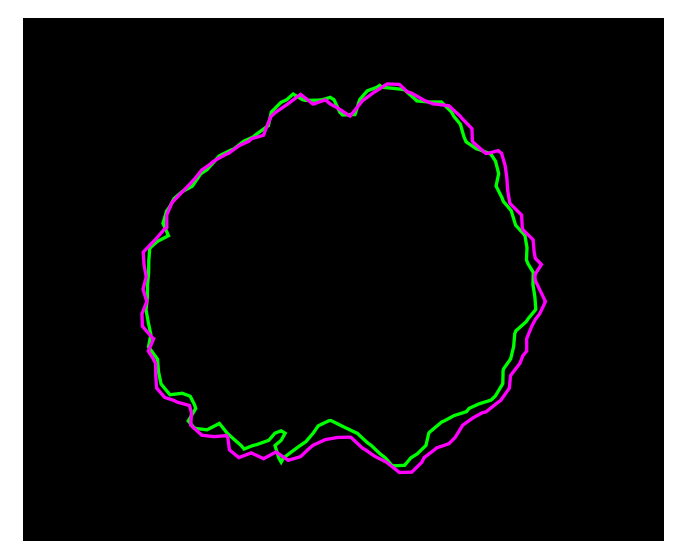


Figure 4. A single contour, marking the edge of the remnant in each epoch, with epoch 1 in green, and epoch 2 in magenta. The contours are smoothed with a 2-pixel Gaussian.

We drew a single contour in ds9 around the remnant in both epochs. Because the vast majority of background pixels in a given Chandra observation have zero counts, a single contour defining the edge of the emission from the remnant (and some small amount of leakage resulting from the wings of the PSF) is quite easy to define, simply be defining a contour level of "1." The contours from both epochs are shown in Figure 4. We converted these contour to region files, and measured the number of pixels contained within each. In the 1999 epoch, this contour contained 2846 pixels, while in 2017 the remnant occupied 2983 pixels. As the area of the remnant increases as the square of the radius, this means that, on average, the radius of the remnant has increased by 2.37%, or about 0.36 pixels. This corresponds to a shock velocity of 4810 km s⁻¹. This is somewhat higher than our average, reported above, but well within the uncertainties, confirming the expansion between the two epochs.

A high shock velocity confirms N103B's status as a young SNR, as reported by Rest et al. (2005) and Lewis et al. (2003). An expansion velocity of 4170 km s⁻¹ implies an undecelerated age for N103B of 850 years, making the real age somewhat lower. It is somewhat surprising to find such a high shock velocity, given the high densities reported in W14. The most obvious caveat here is that by only measuring the change in the remnant's diameter, we cannot know if one side of the remnant is expanding faster than the other. The high densities reported in W14 came from the western half of N103B, the same half in which Ghavamian et al. (2017) reported lower shock velocities from the broad $H\alpha$ component. However, these Balmer line filaments are quite faint, and it is likely that only shocks in denser regions are spectroscopically detectable through their broad component. X-ray emission above 1.7 keV is dominated by intermediate-mass elements, particularly Si and S. If these lines result from the ejecta, their velocity might be different from the blast wave velocity, complicating the results. Thus, to ensure an "apples-to-apples" comparison between the shock velocity implied by the broad $H\alpha$ width and the velocity measured by proper motion, we would need to measure the optical proper motion of the $H\alpha$ filaments used, requiring a second epoch of optical imaging. Optical proper motion measurements could also in principle provide a measure of the deceleration parameter, θ , further constraining the age of the remnant.

A comparison can be drawn here between N103B and *Kepler*'s SNR, where the forward shock speeds are found to vary by about a factor of two between the north and south rims (Katsuda et al. 2008; Vink 2008). If the same velocity ratio is present here (in an east—west direction), that would lead to a shock velocity of \sim 2800 km s⁻¹ in the west (much closer to the speeds seen in Ghavamian et al. 2017) and \sim 5500 km s⁻¹ in the east. Such high shock velocities in N103B may imply a nonthermal synchrotron component in the X-ray spectrum, as is seen in *Kepler*. In a follow-up paper on detailed X-ray spectroscopy, we will explore the evidence for this component.

4. Conclusions

We re-observed the bright LMC SNR N103B with Chandra in 2017, 17.4 years after it was first observed in 1999 with the goal of measuring the expansion of the remnant. The lack of strong detections of point sources in the field of view made absolute alignment of the two epochs impossible, but we were able to measure the change in the diameter of the remnant in four different directions, yielding an average expansion of the shock front of just under $4200 \,\mathrm{km \, s}^{-1}$. This further supports the view that this remnant is young. The undecelerated age is 850 years, but because some deceleration has almost certainly occurred, the real age is younger than this; this is entirely consistent with the estimates from light echo studies (Rest et al. 2005). We encourage future monitoring of this object at all wavelengths, particularly X-ray and optical, where highresolution observations can continue to refine measurements of the expansion.

We thank the anonymous referee for providing valuable comments that improved the manuscript. Support for this work was provided by the National Aeronautics and Space Administration through *Chandra* Award Number G06-17064 issued by the *Chandra* X-ray Center, which is operated by the Smithsonian Astrophysical Observatory for and on behalf of the National Aeronautics Space Administration under contract

NAS8-03060. P.F.W. acknowledges additional support from NSF, through grant AST-1714281. I.R.S. acknowledges support from the Australian Research Council Grant FT160100028.

ORCID iDs

Brian J. Williams https://orcid.org/0000-0003-2063-381X William P. Blair https://orcid.org/0000-0003-2379-6518 Parviz Ghavamian https://orcid.org/0000-0002-9886-0839 Knox S. Long https://orcid.org/0000-0002-4134-864X Robert Petre https://orcid.org/0000-0003-3850-2041 John C. Raymond https://orcid.org/0000-0002-7868-1622 Stephen P. Reynolds https://orcid.org/0000-0002-5365-5444

Ivo R. Seitenzahl https://orcid.org/0000-0002-5044-2988

References

Badenes, C., Harris, J., Zaritsky, D., & Prieto, J. L. 2009, ApJ, 700, 727 Ghavamian, P., Seitenzahl, I. R., Vogt, F. P. A., et al. 2017, ApJ, 847, 122 Helder, E. A., Kosenko, D., & Vink, J. 2010, ApJL, 719, 140 Henize, K. G. 1956, ApJS, 2, 315 Hovey, L., Hughes, J. P., & Eriksen, K. 2015, ApJ, 809, 119 Hughes, J. P., Hayashi, I., Helfand, D., et al. 1995, ApJ, 444, 81 Hughes, J. P., Rakowski, C. E., & Decourchelle, A. 2000, ApJ, 543, 61 Katsuda, S., Long, K. S., Petre, R., et al. 2013, ApJ, 763, 85 Katsuda, S., Tsunemi, H., & Mori, K. 2008, ApJ, 678, 35 Katsuda, S., Tsunemi, H., Uchida, H., & Kimura, M. 2008, ApJ, 689, 225 Kim, M., Kim, D.-W., Wilkes, B. J., et al. 2007, ApJS, 169, 401 Lewis, K. T., Burrows, D. N., Hughes, J. P., et al. 2003, ApJ, 582, 770 Li, C.-J., Chu, Y.-H., Gruendl, R. A., et al. 2017, ApJ, 836, 85 Lopez, L. A., Ramirez-Ruiz, E., Huppenkothen, D., Badenes, C., & Pooley, D. A. 2011, ApJ, 732, 114 Mathewson, D. S., & Clarke, J. N. 1973, ApJ, 180, 725 Patnaude, D. J., Badenes, C., Park, S., & Laming, M. J. 2012, ApJ, 756, 6 Pietrzynski, G., Graczyk, D., Gieren, W., et al. 2013, Natur, 495, 76 Rest, A., Suntzeff, N. B., Olsen, K., et al. 2005, Natur, 438, 1132 Roper, Q., Filipovic, M., Allen, G. E., et al. 2018, MNRAS, 479, 1800 Vink, J. 2008, ApJ, 689, 231 Williams, B. J., Borkowski, K. J., Reynolds, S. P., et al. 2012, ApJ, 755, 3 Williams, B. J., Borkowski, K. J., Reynolds, S. P., et al. 2014, ApJ, 790, 139 Williams, B. J., Coyle, N. M., Yamaguchi, H., et al. 2017, ApJ, 842, 28 Yang, X. J., Tsunemi, H., Lu, F. J., et al. 2013, ApJ, 766, 44